Journal of Power Sources 217 (2012) 543–553

Contents lists available at SciVerse ScienceDirect

Journal of Power Sources

journal homepage: www.elsevier.com/locate/jpowsour

Nanostructured ruthenium – gadolinia-doped ceria composite anodes for thin film solid oxide fuel cells

Yuto Takagi [a,b,*], Suhare Adam [a], Shriram Ramanathan [a]

[a] Harvard School of Engineering and Applied Sciences, Harvard University, Cambridge, MA 02138, USA
[b] Advanced Material Laboratories, Sony Corporation, Atsugi, Kanagawa 243-0021, Japan

HIGHLIGHTS

- Thin film micro-SOFCs with Ru–CGO composite anodes were fabricated.
- Thermal stability of Ru–CGO composite thin film was examined against Ru metal film.
- Power density of 275 mWcm^{-2} at 485 °C was obtained with weakly humidified methane fuel.
- Microstructural stability of Ru–CGO anode is discussed.

ARTICLE INFO

Article history:
Received 10 April 2012
Received in revised form
14 June 2012
Accepted 16 June 2012
Available online 23 June 2012

Keywords:
Electrode
Ruthenium
Solid oxide fuel cells
Thin films
Methane
Gadolinia doped ceria

ABSTRACT

Ruthenium and gadolinia-doped ceria (Ru–CGO) composite nano-crystalline thin film anodes are demonstrated for the first time in self-supported micro-solid oxide fuel cells (μSOFCs) for direct methane utilization, targeting development of microstructurally stable anodes under operation. Nano-composite thin film anodes are synthesized by co-sputtering from Ru metal and CGO oxide targets. Detailed electrical, crystalline and microstructural analyses were carried out on composite films to characterize properties as a function of Ru/CGO relative fraction. Microstructural stability of the composite film is compared to Ru metal film from conductivity and grain size behavior during 500 °C thermal treatments. Stress-relaxed composite thin film anodes were developed on self-supported μSOFCs with yttria-stabilized zirconia thin film electrolytes and porous platinum cathodes. μSOFCs were tested with room temperature humidified methane as fuel and air as the oxidant, exhibited an open circuit voltage of 0.97 V and a peak power density of 275 mW cm^{-2} at 485 °C. Microstructural stability of Ru–CGO composite anodes relative to metal electrodes is discussed. The results suggest a general approach to synthesis of functional metal-oxide nano-composite thin films for electrodes in fuel cells and related energy conversion devices.

1. Introduction

Solid oxide fuel cells (SOFCs) are known for their high power densities and conversion efficiencies [1–4]. Direct operation of SOFCs with hydrocarbons could substantially simplify system complexity and reduce overall cost, and anodes for this purpose have been investigated to date. For example, Park et al. reported direct oxidation of various hydrocarbons with copper-ceria composite anodes at 700–800 °C [5]. Hibino et al. demonstrated a direct methane-fueled SOFC with performance of 750 mW cm^{-2} at 600 °C by utilizing Ni–CGO–Ru anodes [6]. Reducing fuel cell operation temperature to intermediate range would allow a wider range of material choices, rapid start-ups and shutdowns, and reduced energy consumption for start-ups. Thicknesses of electrolyte membranes in thin film SOFCs can be decreased down to nanometric regime, lowering specific resistance of the electrolyte and reducing the operation temperature. For example, Kerman et al. demonstrated a power density of 1.04 W cm^{-2} at 500 °C by optimizing nano-porous platinum (Pt) anode morphology [7]. Operation, performance and properties of low temperature thin film SOFCs utilizing hydrocarbons as fuels have received less attention. Lai et al. demonstrated a power density of 385 mW cm^{-2} at 550 °C with palladium (Pd) anodes, with weakly humidified methane as a fuel [8]. However, the Pd anodes may suffer carbon deposition, which can potentially hinder overall cell performance.

* Corresponding author. Harvard School of Engineering and Applied Sciences, Harvard University, Cambridge, MA 02138, USA. Tel.: +1 6172337863; fax: +1 6174959837.
E-mail addresses: ytakagi@seas.harvard.edu (Y. Takagi), saadam@fas.harvard.edu (S. Adam), shriram@seas.harvard.edu (S. Ramanathan).

0378-7753/$ – see front matter © 2012 Elsevier B.V. All rights reserved.
http://dx.doi.org/10.1016/j.jpowsour.2012.06.060

In a recent work, we have demonstrated thin film μSOFC with peak performance of 450 mW cm^{-2} and an open circuit voltage of 0.71 V at 500 °C with direct supply of weakly humidified methane as a fuel [9]. Nano-porous ruthenium (Ru) anodes were fabricated by physical vapor deposition on thin film μSOFCs with 8 mol% yttria-stabilized zirconia (YSZ) thin film electrolytes and porous Pt cathodes. No carbon deposition was observed in scanning electron microscopy (SEM) study after fuel cell operation. However, metal electrodes are often morphologically unstable at elevated temperatures. Single phase metal electrodes tend to change their morphology due to agglomeration or dewetting during operation, which degrades the fuel cell performance.

Nano-composite electrodes are expected to restrain metal coarsening by confinement in ceramic networks [10–14]. Past works on thin film composite electrodes were focused on Ni-ceramic composites, ceramic materials being either YSZ or gadolinia-doped ceria (CGO). Noh et al. fabricated nano-porous Ni-YSZ thin film between anode support and thin film electrolyte by pulsed laser deposition (PLD). Maximum power of 145 mW cm^{-2} was obtained at 500 °C with hydrogen fuel [15,16]. Muecke et al. investigated microstructures and electrochemical performance of Ni–CGO films prepared by spray pyrolysis and PLD [17–19]. In this study, Ru–CGO composite thin films prepared by co-sputtering are investigated as fuel cell anodes. CGO has been chosen as the ceramic material to stabilize Ru metal nanostructure. Doped ceria displays mixed ionic and electronic conduction at low oxygen partial pressure and is resistant to carbon deposition [20–24]. It also possesses good catalytic activity for hydrogen and methane oxidation processes [21,25,26]. To the best of our knowledge, this is the first attempt to explore metal-ceramic composite thin film anodes for self-supported thin film SOFCs. We provide a detailed study of electrical, crystal structural properties and microstructural stability of Ru–CGO thin films. Macroscopic structural integrity of Ru–CGO anode μSOFC was achieved developing stress-relaxed composite thin film anodes by co-sputtering, and performance of the μSOFCs was optimized by varying the Ru–CGO anode composition. OCV of 0.97 V and a peak power density of 275 mW cm^{-2} were achieved at 485 °C with room temperature humidified methane as fuel and air as the oxidant. Morphological stability of composite anodes is investigated through microstructural analysis following extended operation of μSOFCs.

2. Experimental details

2.1. Growth and characterizations of pure Ru and CGO thin films

Properties of pure Ru and CGO thin films deposited on 0.5 mm thick single crystalline YSZ <100> (sc-YSZ) substrates (MTI Corp.) were investigated. Ru films were deposited by direct current (DC) sputtering from Ru metal target (purity 99.9%, from AJA International, Inc.) in argon (Ar) environment without substrate heating. Deposition rate dependence on pressure (10–75 mTorr) and target power (50–200 W) was determined, film thicknesses resulting in 15–85 nm range. In-plane electrical conductivity of Ru thin films at room temperature was obtained by four point probe resistivity measurements. CGO thin films were deposited by radio-frequency (RF) sputtering from 10 mol% gadolinium-doped cerium oxide target (purity 99.99%, Plasmaterials, Inc.) in Ar environment without substrate heating. Deposition pressure was varied between 5 and 40 mTorr while target power was varied between 100 and 150 W. Film thicknesses were 25–80 nm. Ru and CGO film thicknesses were estimated by X-ray reflectivity (XRR). XRR and X-ray diffraction (XRD) of thin film samples were carried out with a Bruker D8 X-ray Diffractometer using Cu Kα radiation. Morphology of thin films were investigated using Carl Zeiss Ultra-plus Field Emission SEM.

2.2. Growth and characterizations of Ru–CGO composite thin films

Ru–CGO composite thin films were deposited by co-sputtering from metal Ru target and ceramic CGO target described in the previous section. Single crystal sapphire <0001>, sc-YSZ, Si_3N_4 coated Si (Si_3N_4/Si), and YSZ coated Si_3N_4/Si (YSZ/Si_3N_4/Si) were used as substrates. Sapphire substrates were used for electrical characterization and thickness calibration of the composite films while YSZ/Si_3N_4/Si substrates were used for XRD studies. For the YSZ/Si3N4/Si substrates, ~100 nm thick polycrystalline YSZ thin films were deposited on Si_3N_4/Si substrates to simulate the μSOFC electrolyte surface. Different fractions of Ru in composite films were obtained by varying the DC power of Ru target, while RF power of CGO target was fixed to 100 or 150 W. Based on the deposition rates determined from individual Ru and CGO depositions, nominal Ru/CGO ratios were designed in the range of Ru/CGO = 2/3 to 3/1. XRD, XRR, microstructure and room temperature in-plane electrical conductivity of as-deposited Ru–CGO films were characterized accordingly with the same methods for pure Ru and CGO films. Crystalline structure evolution of composite thin films on YSZ/Si_3N_4/Si substrates was investigated by XRD after annealed at 500 °C for 1 h in 5% hydrogen (H_2)–Ar environment. Chemical composition of the samples were evaluated by analyzing X-ray Photoelectron Spectrometer (XPS) spectra acquired in Surface Science SSX-100, after sputtering the samples for 20 min with Ar to remove surface contaminants.

Temperature dependent in-plane conductivity of the thin films deposited on sapphire substrates with 200 nm thick dense gold contacts was measured in an environmental chamber. DC conductivity measurements were performed between room temperature and 500 °C flowing 5% H_2–Ar gas through the chamber, while the sample temperature was ramped up at the rate of 10 °C min^{-1}. Evolution of thin film morphology was studied with SEM before and after the test.

2.3. Fabrication and measurements of thin film μSOFCs with Ru–CGO composite anodes

Si_3N_4-coated Si substrates of 10 × 10 × 0.5 mm^3 were used for μSOFC fabrication. Each substrate was processed to have nine 200 μm × 200 μm Si_3N_4 membranes. Thin film YSZ electrolytes were deposited by RF sputtering from a Y_2O_3 8%:ZrO_2 92% target in Ar environment with deposition pressure of 5 mTorr and 100 W target power at substrate temperature of 550 °C. Thin film Pt cathodes were deposited on YSZ electrolyte by DC sputtering in Ar environment with deposition pressure of 75 mTorr and 200 W target power without substrate heating, conditions being similar with our previous works [27,28]. Nominal deposition rates of as-deposited YSZ and Pt thin films were estimated by XRR to be ~2 and ~4 nm min^{-1}, respectively. After removing Si_3N_4 layer with reactive ion etching (RIE) using O_2 and CF_4, Ru–CGO composite anodes were deposited on free-standing YSZ-Pt structures. Room temperature humidified 5% H_2/Ar gas was supplied to the anodes of μSOFCs at a flow rate of 50 ml min^{-1} during temperature ramp from 250 to 400 °C. At 400 °C the H_2/Ar gas was turned off and room temperature humidified pure methane gas was fed at a flow rate of 50 ml min^{-1}. The cathodes were exposed to laboratory air. Current collection was done through deposited electrodes. Programmed current–voltage (I–V) measurements were carried out periodically during the temperature ramp. Morphology of Ru–CGO composite anodes was investigated with SEM before and after the fuel cell measurements.

3. Results and discussion

3.1. Characterizations of Ru and CGO thin films

Morphology and conductivity of as-deposited Ru thin films on sc-YSZ substrates grown at different deposition pressure and power are shown in Fig. 1(a) and (b). These Ru films are highly granular and grain size shows strong dependence on deposition parameters. Grain size increases with increasing deposition power or decreasing deposition pressure, though it is also sensitive to film thicknesses. At 10 mTorr, film conductivity is relatively high and increases as deposition power is increased. With higher deposition pressures (40 and 75 mTorr) film conductivity becomes relatively low. As film conductivity is strongly related to film porosity (i.e. increased porosity gives lower conductivity), our observations suggest that deposition pressure from above 40 mTorr leads to more porous films. Fig. 2 presents SEM images of as-deposited CGO thin films grown at different deposition pressures and powers. CGO films tend to exhibit smoother morphology compared to Ru films. The films were rougher when deposition pressure was 10–20 mTorr, but became featureless at 40 mTorr with no grain boundaries distinguishable. Typical grain sizes observed at deposition pressure of 10–20 mTorr were 10–20 nm. Growth rates of Ru and CGO films under various pressures and powers are summarized in Fig. 3.

3.2. Characterizations of Ru–CGO composite thin films

3.2.1. Morphology, crystal structure and chemical compositions

Ru–CGO composite films with nominal volumetric Ru/CGO ratio of 2/3, 1/1, 3/2 and 7/3 (namely, R2C3, R1C1, R3C2 and R7C3, respectively) were prepared with deposition parameters shown in Table 1. R3C2 composite films on single crystal sapphire, sc-YSZ and Si_3N_4/Si substrates showed smooth nano-crystalline morphology with grain sizes of ~10 nm as can be seen in Fig. 4(a)–(c). In contrast, the films on YSZ/Si_3N_4/Si substrate showed highly granular morphology with primary grain sizes of ~10 nm and secondary particles or pillars as large as 70–100 nm as shown in Fig. 4(d). This interesting morphology may be due to the different surface textures of polycrystalline YSZ film from single crystal or amorphous substrates. Similar morphology has been observed in Ni-YSZ co-sputtered films [11]. Changing Ru/CGO ratio from 2/3 to 7/3 in composite films on YSZ/Si_3N_4/Si substrates did not result in noticeable change in the morphology (Fig. 5). Fig. 6(a) shows XRD patterns of room temperature deposited composite films on YSZ/Si_3N_4/Si substrates with various Ru fractions. For pure CGO film, peaks from both CGO film and YSZ underlayer were observed and were consistent with cubic fluorite lattice parameters for CGO and YSZ, respectively. Pure Ru film exhibited XRD pattern of hexagonal structure with a relatively weak <002> peak. Only YSZ related peaks were identified with R2C3 and R1C1 films indicating poor crystallization of Ru and CGO, due to formation of amorphous phase or very-fine-grained polycrystalline structure [29]. With increase of Ru content in the films, Ru related peaks appear as presented in the case of R3C2 and R7C3 films. CGO related peaks were not apparent in as-deposited films within the range of the Ru/CGO ratio in this study. Co-deposition of Ru with CGO seems to hinder formation of CGO crystallites. Past studies on metal-ceramic co-deposited films also indicated similar effects [19,30]. In order to investigate crystalline structure evolution in the composite electrode under fuel cell operating condition, R1C1, R3C2 and R7C3 thin films on YSZ/Si_3N_4/Si substrates were annealed at 500 °C in 5 % H_2–Ar environment for 1 h. As shown in Fig. 6(b), annealed Ru–CGO composite thin films showed CGO related peaks along with enhanced Ru peaks, indicating ionic transport capability in the composite anode. As expected, CGO peaks grew stronger as CGO/Ru ratio was increased. It is interesting to note that CGO <200> peaks were suppressed compared to <111> and <220> peaks, indicating preferential growth of CGO under metal-oxide co-deposition which was not observed in pure CGO growth (Fig. 6(a)).

In order to quantify the atomic composition of CGO and Ru, XPS measurements were performed on the thin films. Relative atomic

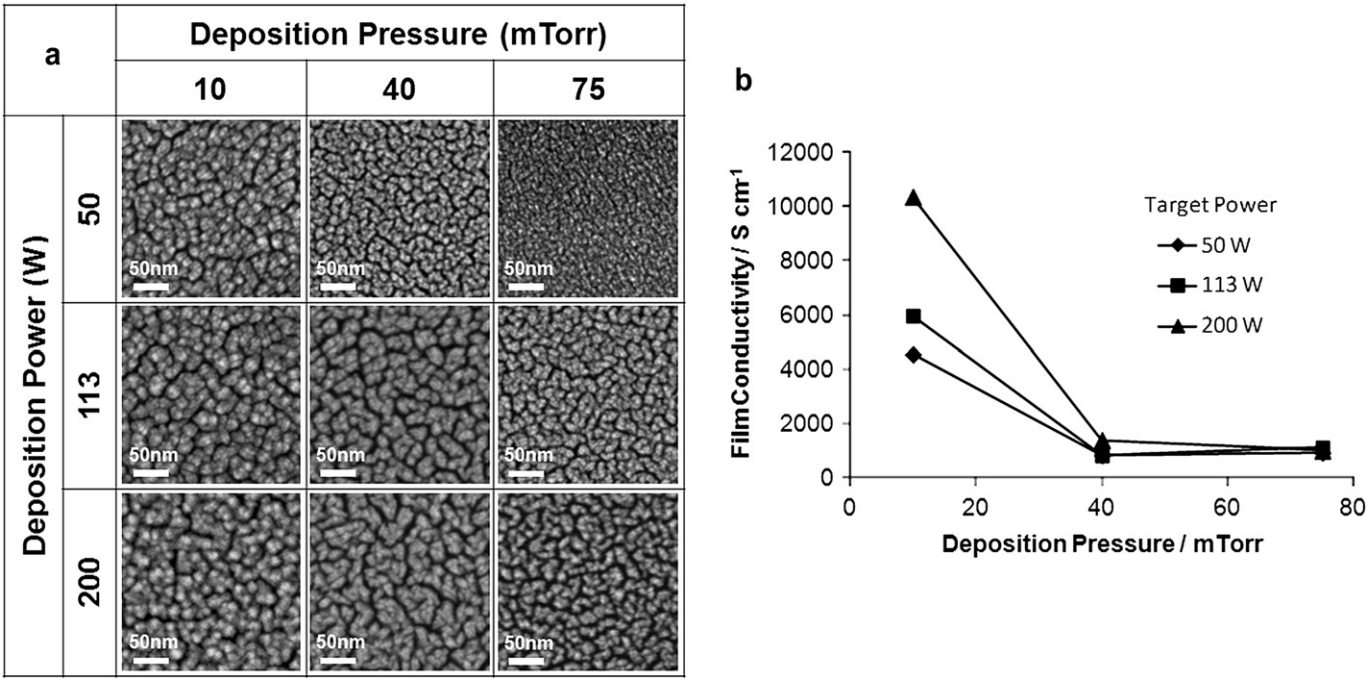

Fig. 1. (a) Surface morphology (SEM) and (b) DC conductivity measured at room temperature of as-deposited Ru films on single crystal YSZ substrates at various deposition pressures and powers. All SEM micrographs are in same scale in (a).

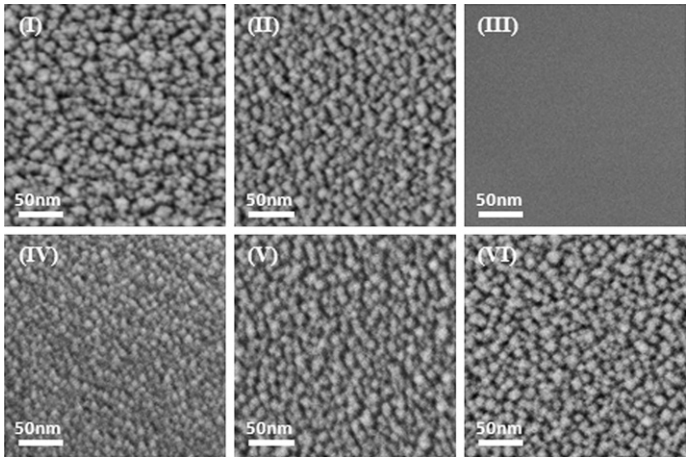

Fig. 2. Surface morphology (SEM) of as-deposited CGO films on single crystal YSZ substrates, at deposition pressures and powers of (I) 10 mTorr, 100 W, (II) 20 mTorr, 100 W, (III) 40 mTorr, 100 W, (IV) 5 mTorr, 150 W, (V) 10 mTorr, 150 W, and (VI) 20 mTorr, 150 W.

molar ratio of Ru to (Ce + Gd) and calculated volumetric ratio of Ru to CGO in R1C1, R3C2 and R7C3 samples are shown in Table 1, respectively. Clear dependency of Ru increase and (Ce + Gd) decrease in film compositions are observed by increasing Ru/CGO nominal deposition ratio from 1/1 to 7/3. The calculated volumetric ratio of Ru to CGO was in fair agreement with those designed from calibrated deposition rates.

3.2.2. Electrical conductivity and stability under thermal treatments

In-plane conductivity of Ru–CGO composite films deposited at 10 mTorr on YSZ/Si_3N_4/Si substrates measured at room temperature is shown in Fig. 7(a). Strong dependence of conductivity on Ru fraction can be observed, implying that in-plane percolating conduction pathways are being developed as Ru content is increased. The high volumetric Ru content of more than 50% required for percolation indicates two-dimensional formation of conduction pathways [31]. Increasing deposition pressure of R7C3 films resulted in lower conductivity as shown in Fig. 7(b) indicating increased film porosity. Temperature dependent in-plane conductivities of a R7C3 film and a pure Ru film deposited on single crystal sapphire substrates were measured in an environmental chamber, flowing 5% H_2–Ar gas constantly to create a reducing environment. As shown in Fig. 8(a), the film conductivity increased from 6.4×10^2 to 1.3×10^3 S cm^{-1} for the R7C3 film, and 1.2×10^3 to 7.7×10^4 S cm^{-1} for the pure Ru film as temperature was ramped up from room temperature to 500 °C. The conductivity of the pure Ru film increased for 6.5 times from the initial state indicating extensive change in metal morphology. The increase in conductivity of the composite film was less than 1/10 compared to the pure metal film, suggesting that the metal-ceramic composite structure effectively restrains Ru coarsening caused by thermal annealing. SEM images before and after the *in-situ* heating tests are compared in Fig. 8(b). As seen in images (II) and (IV), coarsening and growth of Ru grains from <10 nm to 30–40 nm was observed for the pure metal film. The composite film showed no distinguishable change in the morphology as can be seen in images (I) and (III). Grain growth was minor, if any, resulting in ~10 nm grain sizes. Morphology evolutions of Ru and Ru–CGO films through high temperature annealing also suggest that co-sputtered Ru–CGO composite structure effectively stabilizes electrode microstructures.

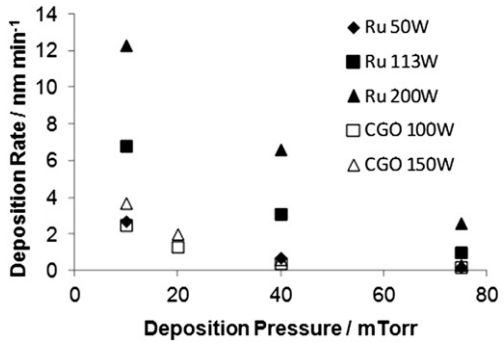

Fig. 3. Dependence of Ru and CGO film deposition rates on deposition pressure and power.

3.3. Characterization of Ru–CGO composite anodes on μSOFCs and fuel cell measurements

3.3.1. Fabrication and performance testing of μSOFCs

Ru–CGO composite anodes were deposited on μSOFCs with various relative fractions. μSOFCs were buckled as a result of compressive film stresses in deposited dense YSZ film, which is typically seen in such membranes (Fig. 9). Fig. 10(a) and (b) shows SEM micrographs of R7C3 and Ru/CGO = 3/1 (namely, R3C1) anodes on μSOFC thin film electrolyte before the fuel cell measurements. Unlike the highly granular Ru–CGO thin films deposited on YSZ/Si_3N_4/Si substrates, Ru–CGO anode films deposited on self-supported electrolytes exhibited a smoother feature. Differences in morphology when depositing anode films on

Table 1
Nominal compositions, deposition conditions, atomic ratios of Ru/(Ce + Gd), and corresponding volumetric ratios of Ru/CGO of composite thin films.

Sample ID	Nominal Ru/CGO ratio by deposition rates	Ru target DC power [W]/CGO target RF power [W]	Deposition pressure [mTorr]	Atomic ratio of Ru/(Ce + Gd) measured by XPS	Volumetric ratio of Ru/CGO[a]
R2C3	2/3	31/100	10	N/A	N/A
R1C1	1/1	46/100	10	79/21	55/45
R3C2	3/2	69/100	10	84/16	65/35
R7C3	7/3	108/100	10	89/11	74/26

[a] Volumetric ratio is estimated under the assumption that CGO is in cubic fluorite phase.

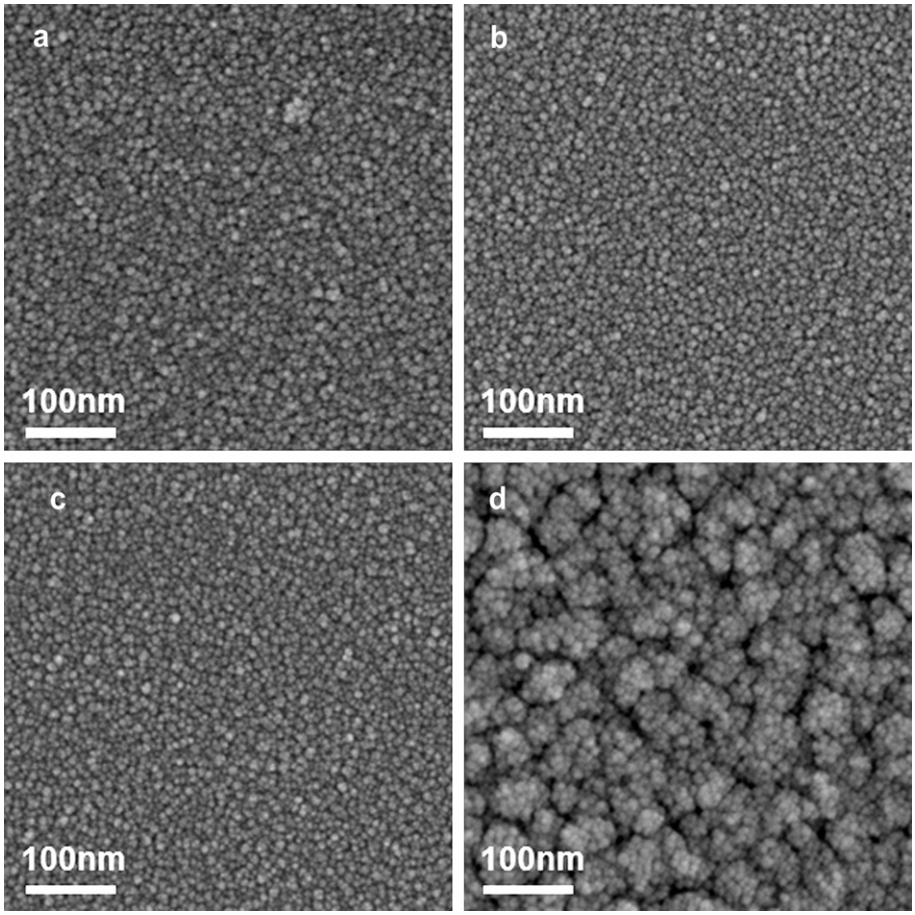

Fig. 4. SEM micrographs of R3C2 composite films on (a) Si_3N_4/Si, (b) single crystal YSZ, (c) single crystal sapphire, and (d) YSZ/Si_3N_4/Si substrates. (R3C2 represents nominal volumetric ratio of Ru/CGO = 3/2.)

a lithographically patterned structure of μSOFCs have been reported in previous works and possibly results from geometrical effects during sputter deposition and low thermal mass of the free-standing electrolyte membranes [8,9,28].

Table 2 summarizes deposition parameters and performance test results of fabricated Ru–CGO anode μSOFCs. Increasing Ru/CGO ratio from 1/1 to 7/3 lead to improvement of OCV under hydrogen fuel, as seen in the test results of FC1, FC2 and FC3. However when cell temperatures were ramped up to ~400 °C, fuel cells with anodes deposited at 10 mTorr mechanically failed by membrane fractures. SEM image of a broken fuel cell (FC3) is shown in Fig. 11(a) exhibiting fractures through the entire membrane. Ceria based electrolytes are known to have mechanical instabilities due to the lattice expansion arising from the transition of Ce^{4+} to Ce^{3+} under reducing conditions [22,23,32,33]. The failures of thin films we have observed may be attributed to this expansion of the anode electrodes. Changing the deposition pressure to 40 mTorr improved the mechanical stability of μSOFCs. Increased deposition pressure is expected to decrease the density of the film, which can in turn relax compressive stresses induced during temperature ramp. Our electrical and microstructural measurement results shown in Sections 3.1 and 3.2 also indicate that Ru and Ru–CGO films deposited at 40 mTorr are less dense compared to the films deposited at 10 mTorr. FC4 and FC5 having anodes deposited at 40 mTorr both survived the temperature ramp followed by fuel switching and generated power with methane fuel. Both FC4 and FC5 exhibited mechanically intact membranes without cracks or fractures after fuel cell operations, as shown in Fig. 11(b). Fuel cell performance measurement results of FC4 and FC5 are shown in Fig. 12(a) and (b). FC4 exhibited maximum power of 31 mW cm^{-2} with OCV of 0.96 V at 500 °C, while those at 455 °C were 19 mW cm^{-2} and 0.89 V, respectively. With higher Ru content, FC5 exhibited maximum power of 275 mW cm^{-2} and an OCV of 0.97 V at 485 °C, while those at 450 °C were 155 mW cm^{-2} and 0.92 V, respectively. To the best of authors' knowledge, these are the first reports of functional self-supported thin film SOFCs with metal-ceramic composite electrodes, and more over, with direct methane fuel feed. The power density at 485 °C is lower than what we have previously observed with nano-porous Ru metal anode μSOFCs [9], but still comparable to the high performance reported to date for methane-fueled fuel cells operated at equivalent temperatures [34]. Increase in OCV observed with operating temperature suggests improved catalytic activity of the electrodes. Improved performance of FC5 compared to FC4 is likely due to the increased catalytic activity of Ru and improved in-plane conductivity for current collection. As shown in Fig. 7(a), in-plane conductivity of the composite electrodes is highly sensitive to the metal fraction. In fact, the Ru/CGO ratio of FC5 anodes (R3C1) is 30% higher than FC4 (R7C3), and R3C1 films deposited at 40 mTorr exhibited 40% higher conductivity than R7C3 films as shown in Fig. 13. These fuel cell test results also indicate that the crystallized CGO in the composite anodes offers ionic transport paths in composite electrodes, and are consistent with the XRD results of post annealed composite films discussed in Section 3.2.

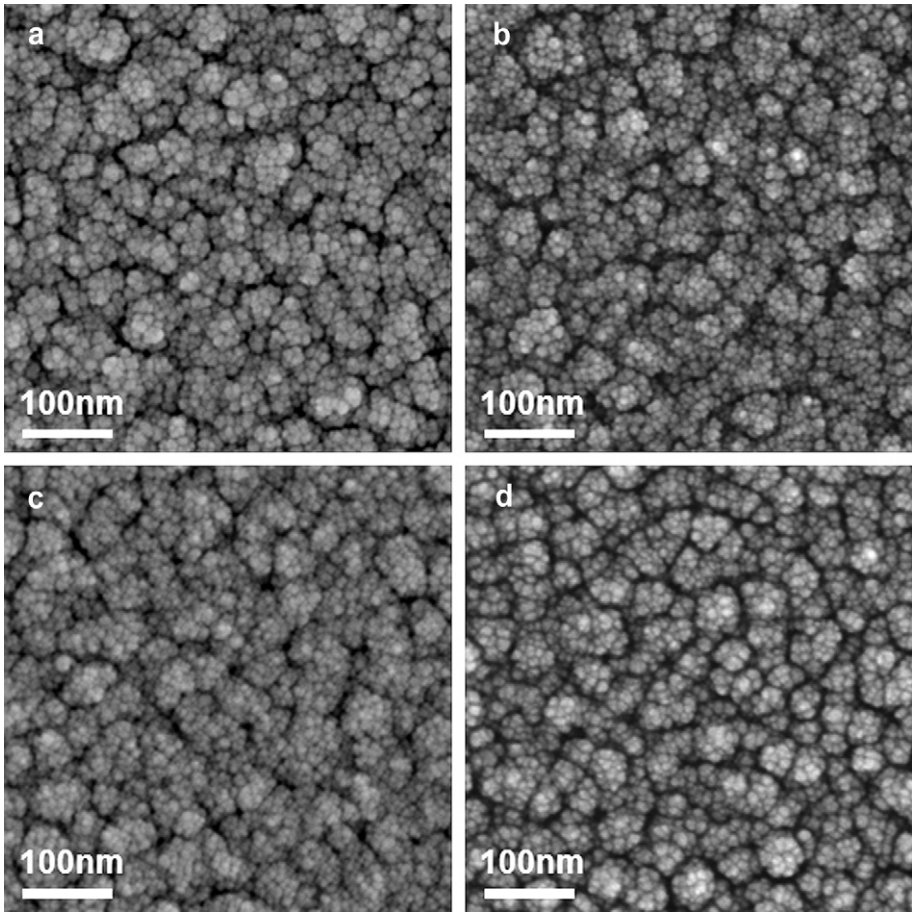

Fig. 5. SEM micrographs of (a) R2C3, (b) R1C1, (c) R3C2, and (d) R7C3 films deposited on YSZ/Si_3N_4/Si substrates, all films exhibit highly granular morphology. (R2C3, R1C1, R3C2, R7C3 represents nominal volumetric ratio of Ru/CGO = 2/3, 1/1, 3/2, 7/3, respectively.)

3.3.2. Extended operation of μSOFCs and microstructural investigations

In order to investigate microstructural stability of the electrodes, FC5 was tested over 3 h by keeping fuel cell at 500 °C under OCV condition, while *I–V* measurements were carried out every 15 min sweeping the cell voltage from 0.85 to 0.35 V and measuring the current. While the length of the test may seem relatively short, the results are expected to provide new insights into the field of thin

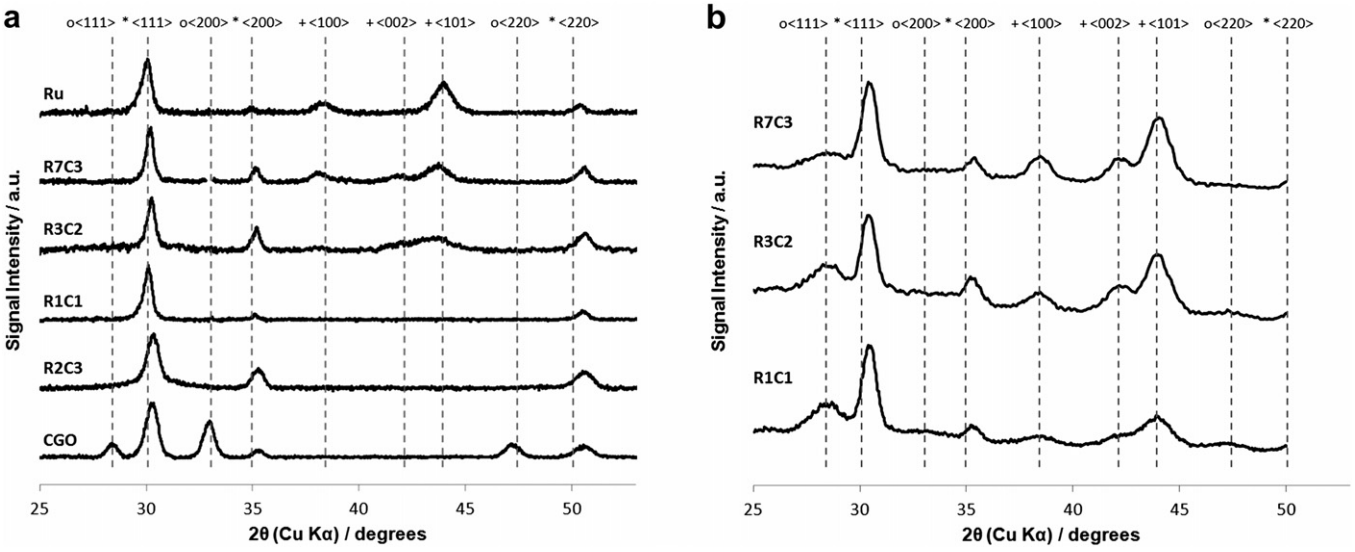

Fig. 6. X-ray diffraction patterns of (a) as-deposited Pure Ru, R7C3, R3C2, R1C1, R2C3, and Pure CGO films on YSZ/Si_3N_4/Si substrates, (b) R7C3, R3C2, and R1C1 films on YSZ/Si_3N_4/Si substrates annealed at 500 °C in 5% H_2–Ar environment for 1 h. Peak positions of (*) cubic YSZ indexed in JCPDS 00-030-1468, (+) hexagonal Ru indexed in JCPDS 01-073-7011, and (○) cubic CGO indexed in JCPDS 00-050-0201 are presented in the figures.

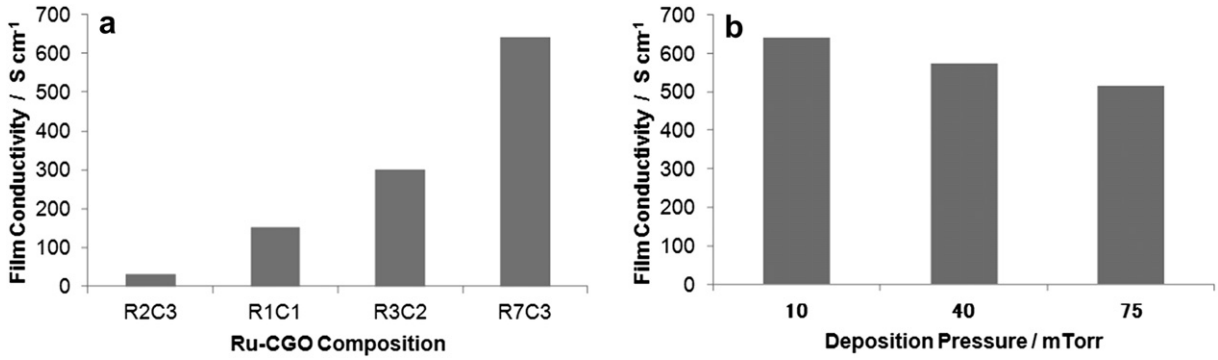

Fig. 7. (a) DC conductivity of 10 mTorr deposited films with different Ru/CGO ratios on single crystal sapphire substrates measured at room temperature. (b) DC conductivity of as-deposited R7C3 films with different deposition pressures, measured at room temperature.

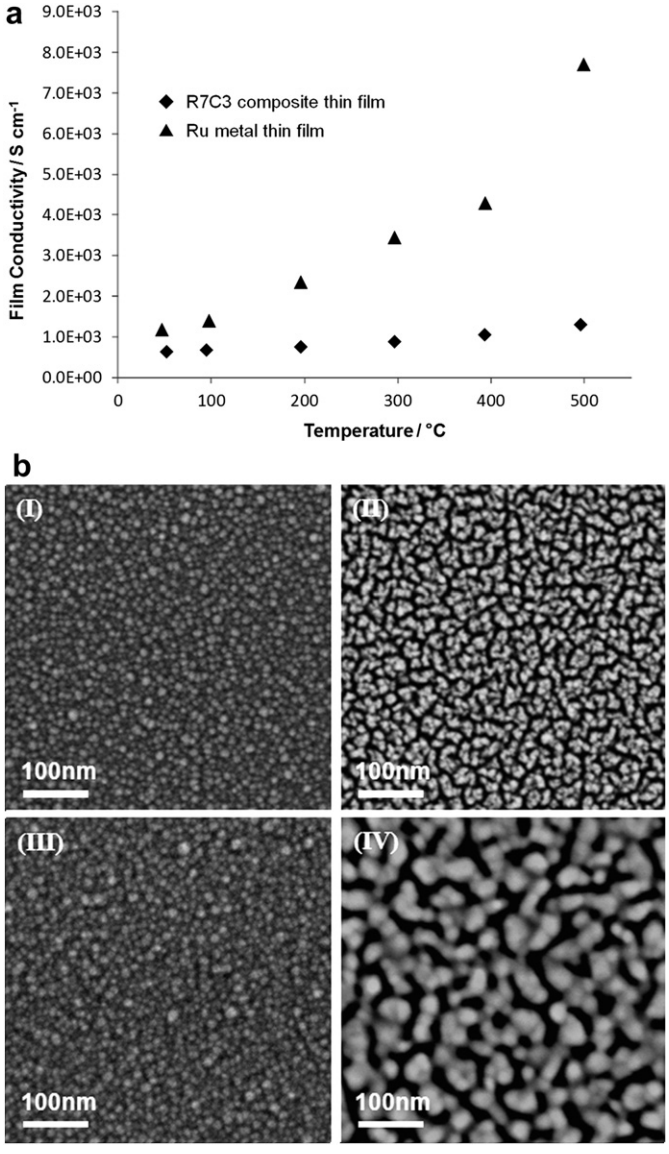

Fig. 8. (a) In-plane conductivity of the R7C3 and Ru metal films deposited on sapphire substrates, measured in-situ under heating from room temperature to 500 °C in 5 % H_2-Ar condition. (b) Surface morphology of films before (I, II), and after (III, IV) the heating test; (I, III) R7C3, and (II, IV) Ru metal film.

film μSOFCs, where very limited studies exist on stability to date. For instance, Kerman et al. performed 12 h test of Pt/YSZ/Pt μSOFCs with hydrogen fuel at 400 °C, and found that the power density decreased by 50% [7]. Degradation was attributed to instability in electrode microstructures. As presented in Fig. 14(a), peak power densities of the fuel cell (FC5) showed good stability for the first 2 h, and decreased to 62% of the initial value after 3 h. Fig. 14(b) shows the current density evolution in the voltage range of 0.6–0.75 V, where SOFCs are expected to operate in order to efficiently convert chemical energy to electrical energy. It is interesting to note that the current decrease at these operating voltages was relatively moderate (~25%) compared to the decrease at peak power.

SEM cross-sectional views of fractured μSOFC (FC5) after extended methane operation were studied to investigate structural integrity of the μSOFC and morphological evolution of the electrodes. Fig. 15(a) focuses on electrolyte, (b) on cathode, and (c) on anode. Note that the thin films are curled after membranes were fractured due to different internal stresses in YSZ electrolytes and Ru-CGO anodes. Good adhesions among Pt cathodes, YSZ electrolytes and Ru–CGO composite anodes were observed. The thickness of YSZ electrolyte was ~100 nm, Ru–CGO anodes and Pt cathodes were 30–40 nm. From the images, it is clearly observed that

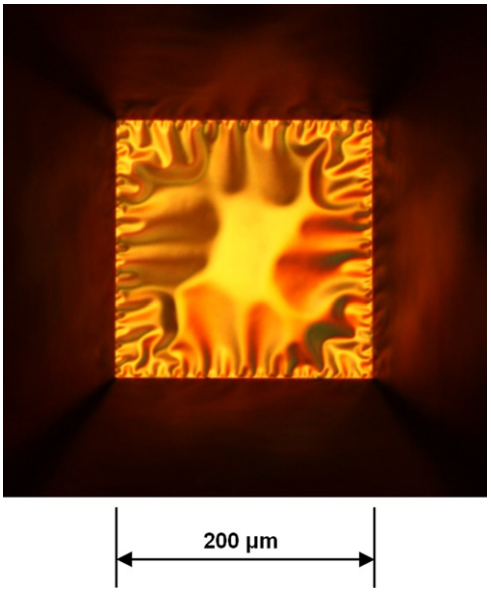

Fig. 9. Optical micrograph of self-supported μSOFC with Ru–CGO composite anode, taken from the anode side. Buckling is due to the compressive stress typical in such membranes.

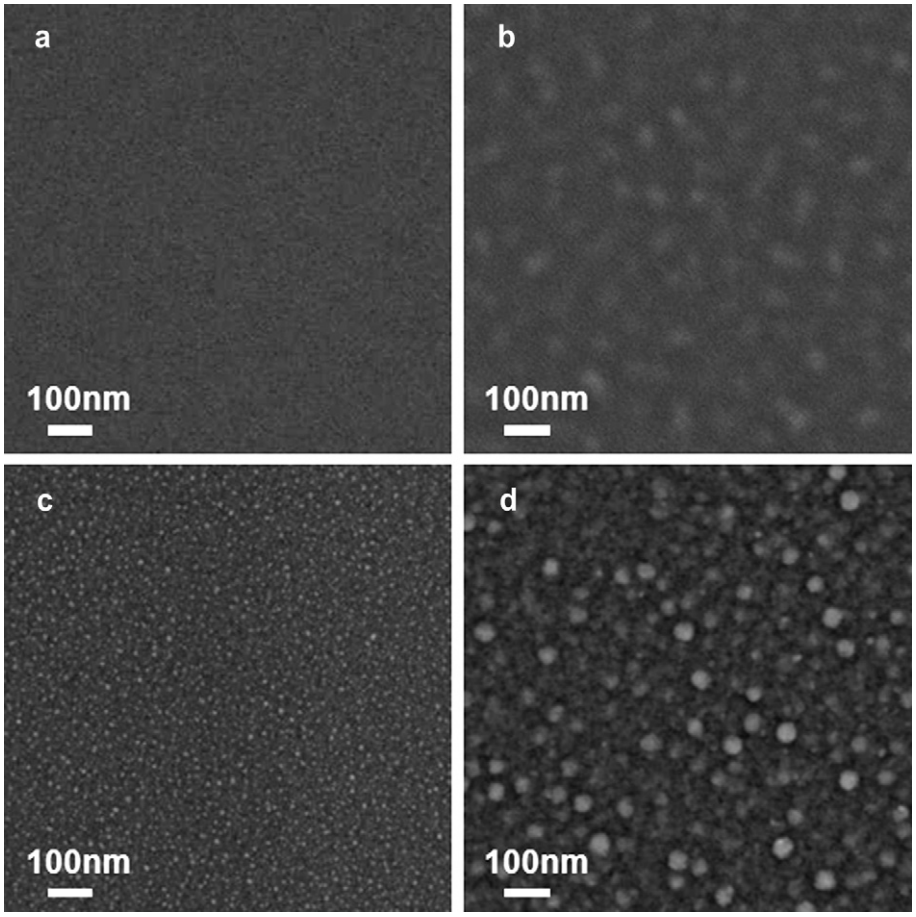

Fig. 10. SEM micrographs of Ru–CGO composite anodes on μSOFCs, as-deposited (a, b), and after fuel cell operations (c, d); (a, c) FC4 with R7C3 anodes, and (b, d) FC5 with R3C1 anodes.

Table 2
Anode compositions, deposition pressures and fuel cell test results of μSOFCs with Ru–CGO composite anodes.

Fuel cell ID	Anode composition	Deposition pressure [mTorr]	OCV with H_2 fuel [V]	OCV with CH_4 fuel [V]	Maximum Power with CH_4 fuel [mW cm^{-2}]
FC1	R1C1	10	0.14	Not measurable	Not measurable
FC2	R3C2	10	0.88	Not measurable	Not measurable
FC3	R7C3	10	0.98	Not measurable	Not measurable
FC4	R7C3	40	1.0	0.96	31
FC5	R3C1	40	0.93	0.99	275

Ru–CGO anodes maintain finer morphology than Pt cathodes, suggesting better microstructural stability. Pure Pt electrodes may experience sintering at temperature above 400 °C and lead to decrease in active area [28,35]. As shown in Fig. 16, Pt cathodes after operation showed morphological deformation and decrease in triple phase boundary length, likely being the cause of performance decay observed.

To take a closer look of morphologies and possible carbon deposition, planar SEM micrographs of composite anodes after the fuel cell tests are shown in Fig. 10(c) for FC4 and (d) for FC5. No visible sign of carbon deposition, such as filaments, sheets or

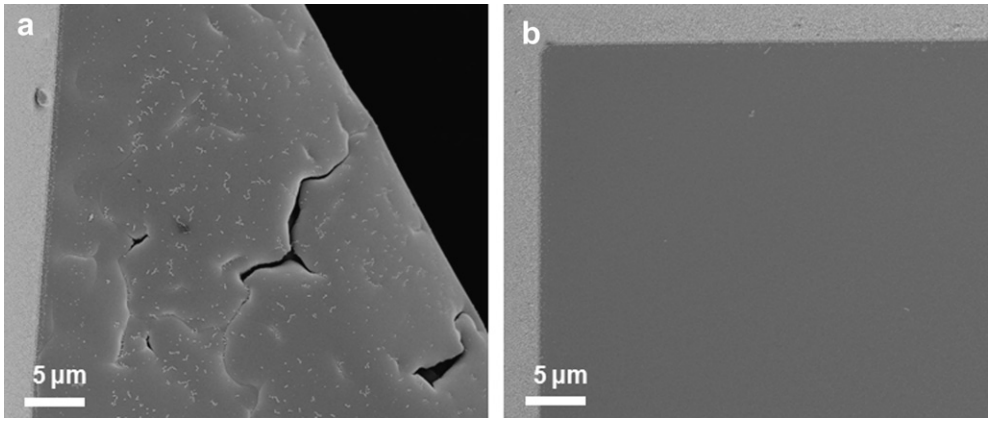

Fig. 11. SEM micrographs of μSOFCs after operation, (a) FC3; anode deposited at 10 mTorr, and (b) FC4; anode deposited at 40 mTorr.

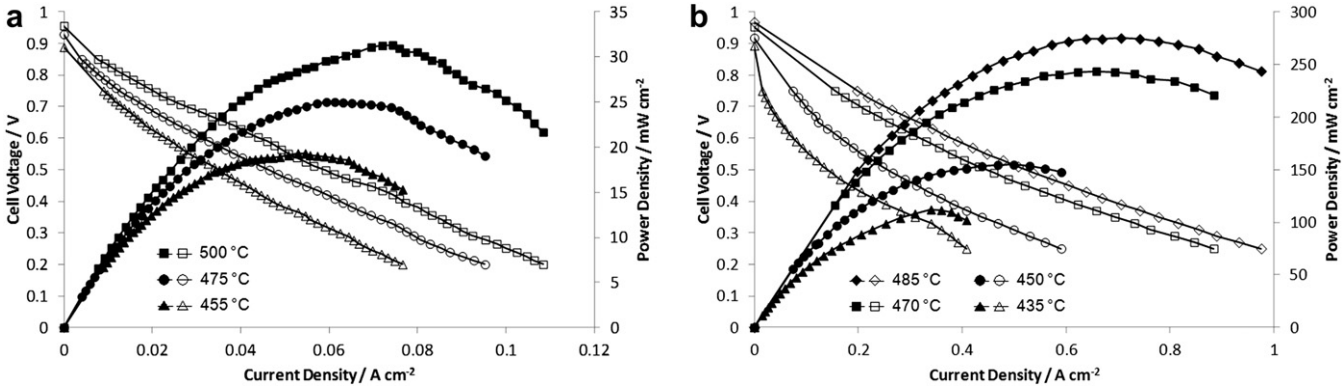

Fig. 12. Performance of Ru–CGO composite anode/YSZ electrolyte/Pt cathode μSOFCs, (a) FC4 and (b) FC5, with room temperature humidified methane as the fuel. The composite anodes are R7C3 for FC4 and R3C1 for FC5. Open and closed symbols represent voltage and power density, respectively.

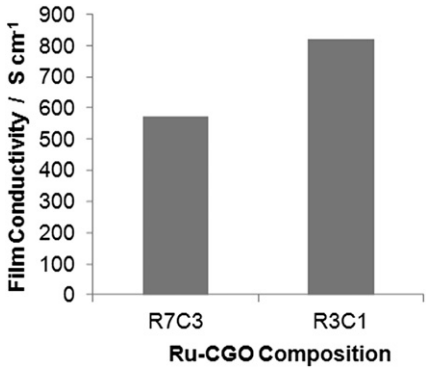

Fig. 13. DC conductivity of 40 mTorr deposited films with different Ru/CGO ratios on single crystal sapphire substrates measured at room temperature.

crystals was observed, as consistent with previous results with pure Ru metal anodes [9]. Trace carbon existence on the electrode surface may not be captured by SEM, however, if carbon deposition at the level that degrades fuel cell performance exists, macroscopic evidence would be expected. Ru is known to be catalytically active for steam and dry reforming [36–38], and also highly resistant to carbon depositions. The local coupling of these reforming reactions and its characteristics allow electrochemical reaction products, H_2O and CO_2, to be utilized in chemically converting methane to H_2 and CO. These species may be consumed as fuels and generate H_2O and CO_2, which can further aid reforming and accelerate the overall number of reactions [39]. Compared to the SEM micrographs of the anodes before fuel cell tests (Fig. 10(a) and (b) for FC4 and FC5, respectively), the grain boundaries became clearer in both FC4 and FC5 anodes. Grain sizes after fuel cell operation were ~10 nm for FC4 and ~40 nm for FC5, not noticeably different from the initial sizes. This indeed indicates improved microsturctural stability of Ru–CGO composite anodes compared to pure Ru metal anodes [9] and composite thin film anodes studied to date. It has been reported that in co-deposited Ni–YSZ composite electrodes, Ni particles can grow from <50 nm to the order of 300–500 nm in reducing atmosphere at elevated temperatures [16,18]. The microstructural stability of the Ru–CGO composite anodes can be attributed to following reasons; the Ru–CGO electrodes are designed to be less porous, whereas Ni-ceramic electrodes in previous studies are intended to be porous by reduction of NiO to Ni. Denser composite films likely have more stable nanostructure, inhibiting agglomeration of metal particles in open pores. Moreover, denser electrodes have less compressive stress transfer to electrolytes during volume shrinkage accompanied by reduction of oxidized metal, which is a critical factor when fabricating composite electrodes on self-supported thin film electrolytes. Additionally, Ru is expected to have better microstructural stability compared to Ni due to its higher melting point (Ru: 2334 °C, Ni: 1455 °C). Finally, thin film electrolytes in μSOFCs allow reduced operation temperature, which suppresses metal agglomeration in the electrode.

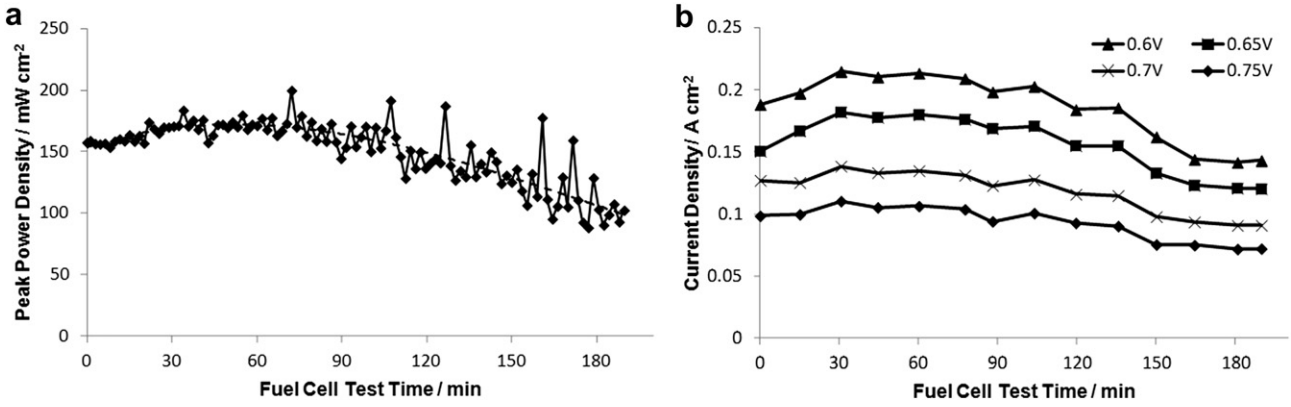

Fig. 14. (a) Evolution of maximum power density during extended operation of FC5 at 500 °C. (b) Current density evolution at different cell voltages during the extended operation.

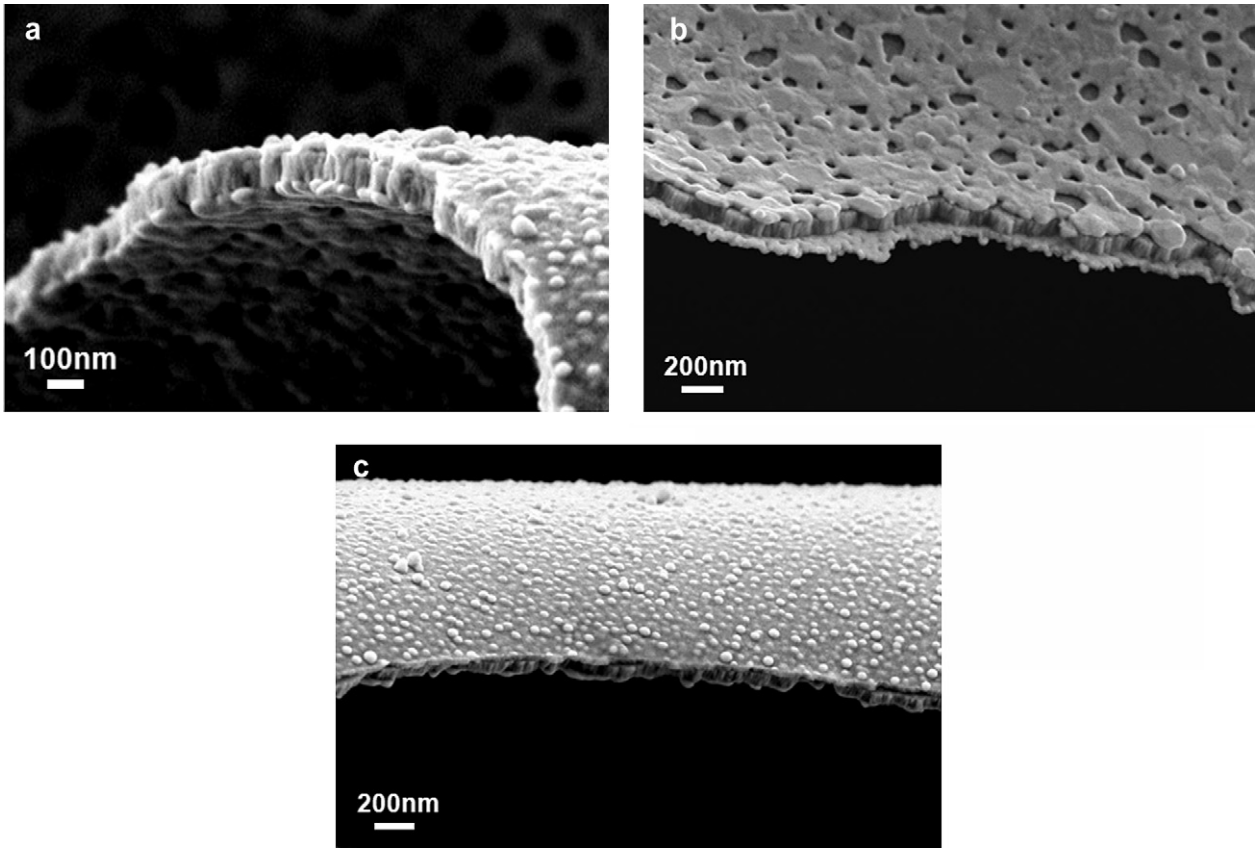

Fig. 15. SEM cross-sectional views of FC5 after extended fuel cell operation focused on (a) YSZ electrolyte, (b) Pt cathode, and (c) Ru–CGO composite anode.

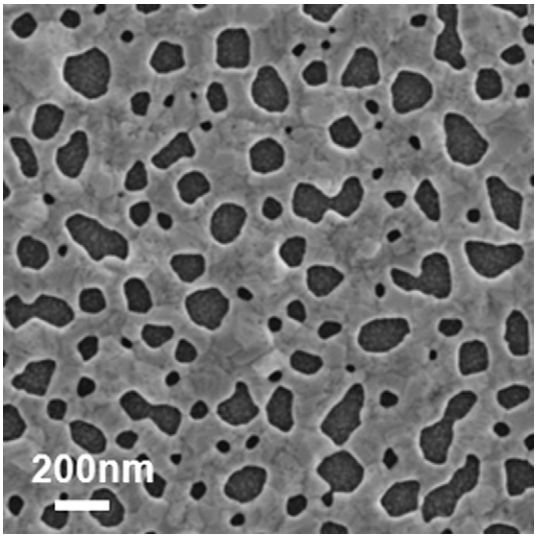

Fig. 16. SEM micrograph of Pt cathode on FC5 after extended fuel cell operation.

4. Conclusions

Thin film μSOFCs with Ru–CGO composite thin film anodes, YSZ electrolytes, and Pt cathodes have been fabricated and tested for direct methane utilization. DC in-plane conductivity and crystalline structure of composite films were investigated for various relative fractions of the metal and oxide. The composite film showed better microstructural stability than the Ru film, where its conductivity change during heating to 500 °C was 1/10 of that of Ru film with no apparent morphological change. The CGO phase in the composite film was crystalline after the annealing, indicating ionic transport capability in the composite electrode. Fuel cells with stress-relaxed Ru–CGO composite anodes were operated with room temperature humidified methane as fuel and air as the oxidant. An open circuit voltage of 0.97 V and a peak power density of 275 mW cm^{-2} were achieved at 485 °C. Analysis following extended fuel cell operation indicated improved microstructural stability of Ru–CGO composite anodes relative to Ru metal anodes and Pt cathodes. The results presented here are of relevance in advancing metal-oxide nanocomposite thin film electrodes for next generation energy conversion and storage devices.

Acknowledgments

We are grateful to National Science Foundation Grant CCF-0926148 and SONY Corporation for financial support. The authors thank Kian Kerman and Quentin Van Overmeere for valuable discussions.

References

[1] E.P. Murray, T. Tsai, S.A. Barnett, Nature 400 (1999) 649–651.
[2] Z.P. Shao, S.M. Haile, J. Ahn, P.D. Ronney, Z.L. Zhan, S.A. Barnett, Nature 435 (2005) 795–798.
[3] T. Hibino, A. Hashimoto, M. Yano, M. Suzuki, M. Sano, Electrochimica Acta 48 (2003) 2531–2537.
[4] S. McIntosh, J.M. Vohs, R.J. Gorte, Electrochemical and Solid-State Letters 6 (2003) A240–A243.
[5] S.D. Park, J.M. Vohs, R.J. Gorte, Nature 404 (2000) 265–267.
[6] T. Hibino, A. Hashimoto, K. Asano, M. Yano, M. Suzuki, M. Sano, Electrochemical and Solid-State Letters 5 (2002) A242–A244.

[7] K. Kerman, B.K. Lai, S. Ramanathan, Journal of Power Sources 196 (2011) 2608–2614.
[8] B.-K. Lai, K. Kerman, S. Ramanathan, Journal of Power Sources 196 (2011) 6299–6304.
[9] Y. Takagi, B.K. Lai, K. Kerman, S. Ramanathan, Energy & Environmental Science 4 (2011) 3473–3478.
[10] E. Rezugina, A.L. Thomann, H. Hidalgo, P. Brault, V. Dolique, Y. Tessier, Surface and Coatings Technology 204 (2010) 2376–2380.
[11] S. Jou, T.H. Wu, Journal of Physics and Chemistry of Solids 69 (2008) 2804–2812.
[12] G.J. La, J. Hertz, H. Tuller, Y. Shao-Horn, Journal of Electroceramics 13 (2004) 691–695.
[13] L.S. Wang, S.A. Barnett, Solid State Ionics 61 (1993) 273–276.
[14] T. Tsai, S.A. Barnett, Solid State Ionics 98 (1997) 191–196.
[15] H.S. Noh, J.W. Son, H. Lee, H.S. Song, H.W. Lee, J.H. Lee, Journal of Electrochemical Society 156 (2009) B1484–B1490.
[16] H.S. Noh, J.W. Son, H. Lee, H.I. Ji, J.H. Lee, H.W. Lee, Journal of the European Ceramic Society 30 (2010) 3415–3423.
[17] U.P. Muecke, K. Akiba, A. Infortuna, T. Salkus, N.V. Stus, L.J. Gauckler, Solid State Ionics 178 (2008) 1762–1768.
[18] U.P. Muecke, S. Graf, U. Rhyner, L.J. Gauckler, Acta Materialia 56 (2008) 677–687.
[19] A. Infortuna, A.S. Harvey, U.P. Muecke, L.J. Gauckler, Physical Chemistry Chemical Physics 11 (2009) 3663–3670.
[20] H. Timmermann, D. Fouquet, A. Weber, E. Ivers-Tiffee, U. Hennings, R. Reimert, Fuel Cells 6 (2006) 307–313.
[21] J. Mermelstein, M. Millan, N. Brandon, Journal of Power Sources 195 (2010) 1657–1666.
[22] V.V. Kharton, F.M.B. Marques, A. Atkinson, Solid State Ionics 174 (2004) 135–149.
[23] W.Z. Zhu, S.C. Deevi, Materials Science and Engineering A – Structural Materials Properties Microstructure and Processing 362 (2003) 228–239.
[24] D.J.L. Brett, A. Atkinson, D. Cumming, E. Ramirez-Cabrera, R. Rudkin, N.P. Brandon, Chemical Engineering Science 60 (2005) 5649–5662.
[25] M. Lo Faro, D. La Rosa, G. Monforte, V. Antonucci, A.S. Arico, P. Antonucci, Journal of Applied Electrochemistry 37 (2007) 203–208.
[26] O.A. Marina, M. Mogensen, Applied Catalysis A: General 189 (1999) 117–126.
[27] B.K. Lai, A.C. Johnson, M. Tsuchiya, S. Ramanathan, Proceedings of SPIE 7679 (2010) 767916-1–767916-6.
[28] A.C. Johnson, B.K. Lai, H. Xiong, S. Ramanathan, Journal of Power Sources 186 (2009) 252–260.
[29] T. Tsai, S.A. Barnett, Journal of Vacuum Science & Technology A 13 (1995) 1073–1077.
[30] J.L. Hertz, H.L. Tuller, Journal of Electrochemical Society 154 (2007) B413–B418.
[31] P. Sotta, D. Long, The European Physical Joural E 11 (2003) 375–387.
[32] D.J.L. Brett, A. Atkinson, N.P. Brandon, S.J. Skinner, Chemical Society Reviews 37 (2008) 1568–1578.
[33] M. Mogensen, S. Primdahl, M.J. Jorgensen, C. Bagger, Journal of Electroceramics 5 (2000) 141–152.
[34] T. Suzuki, T. Yamaguchi, K. Hamamoto, Y. Fujishiro, M. Awano, N. Sammes, Energy & Environmental Science 4 (2011) 940–943.
[35] X.H. Wang, H. Huang, T. Holme, X. Tian, F.B. Prinz, Journal of Power Sources 175 (2008) 75–81.
[36] M.J. Hei, H.B. Chen, J. Yi, Y.J. Lin, Y.Z. Lin, G. Wei, D.W. Liao, Surface Science 417 (1998) 82–96.
[37] D. Qin, J. Lapszewicz, Catalysis Today 21 (1994) 551–560.
[38] M.J. Saeki, H. Uchida, M. Watanabe, Catalysis Letters 26 (1994) 149–157.
[39] J.T.S. Irvine, A. Sauvet, Fuel Cells 1 (2001) 205–210.